"Submitted for publication as part of the special issue on The Materials Chemistry of Energy Conversion"

Rational synthesis and characterization of a new family of low thermal conductivity misfit layer compounds $[(PbSe)_{0.99}]_m(WSe_2)_n$

*Qiyin Lin[1], Mary Smeller[2], Colby L. Heideman[2], Paul Zschack[3], Mikio Koyano[4], Michael D. Anderson[2,6], Robert Kykyneshi,[5] Douglas A. Keszler,[5] Ian M. Anderson[6] and David C. Johnson[2]**

1. Department of Physics, University of Oregon 1253 University of Oregon, Eugene, OR 97403
2. Department of Chemistry, University of Oregon 1253 University of Oregon, Eugene, OR 97403
3. Advanced Photon Source, Argonne National Laboratory, Argonne, IL 60439
4. School of Materials Science, Japanese Institute of Advanced Science and Technology, Ishikawa, Japan, 923-1292
5. Department of Chemistry, Oregon State University, 153 Gilbert Hall, Corvallis, OR 97331-4003
6. Surface and Microanalysis Science Division, National Institute of Standards and Technology, 100 Bureau Dr, Stop 8371, Gaithersburg, MD 20899

Abstract

We describe here a general synthesis approach for the preparation of new families of misfit layer compounds and demonstrate its effectiveness through the preparation of the first 64 members of the $[(PbSe)_{0.99}]_m(WSe_2)_n$ family of compounds, where *m* and *n* are integers that were systematically varied from 1 to 8. The new compounds $[(PbSe)_{1+y}]_m(WSe_2)_n$ were synthesized by annealing reactant precursors containing *m* layers of alternating elemental Pb and Se followed by *n* layers of alternating elemental W and Se, in which the thickness of each pair of elemental layers was calibrated to yield a structural bilayer of rock salt structured PbSe and a trilayer of hexagonal WSe_2. The compounds are kinetically trapped by the similarity of the composition profiles and modulation lengths in the precursor and the targeted compounds. The structural evolution from initial reactant of layer elements to crystalline misfit layer compounds was tracked using X-ray diffraction. The crystal structures of new compounds were probed using both analytical electron microscopy and X-ray diffraction. The c-axis of the misfit layer compound is perpendicular to the substrate, with a c-axis lattice parameter that changes linearly with a slope of (0.612 to 0.615) nm as *m* is changed and *n* is held constant and with a slope of (0.654 to 0.656) nm as *n* is varied and *m* is held constant. The in-plane lattice parameters did not change as the individual layer thicknesses were increased and a misfit parameter of $y = -0.01$ was calculated, the first negative misfit parameter among known misfit layer compounds,. Analytical electron microscopy images and X-ray diffraction data collected on mixed *hkl* reflections revealed rotational (turbostratic) disorder of the a-b planes.

Introduction

The year 2008 spike in energy costs resulted in a renewed focus on increasing the efficiency of energy use and the development of high-efficiency energy conversion and renewable energy technologies to reduce the world's dependence on fossil fuels.[1, 2] The development of new materials with low thermal conductivity is critical to conserving energy and to improving the efficiency of energy conversion technologies. For example, more effective thermal barrier coatings for heat engines increase efficiency by reducing energy dissipation[3-5] and the efficiency of thermoelectric materials[6-8] that convert waste heat into electrical energy increases as thermal conductivity decreases.

Recently an extraordinarily low thermal conductivity of (0.03 to 0.05) $W \cdot m^{-1}K^{-1}$ was reported for a fully

dense material - a disordered form of WSe_2.[9] The low thermal conductivity was attributed to a very short coherence length between the Se-W-Se dichalcogenide layers due to rotational disorder between the layers. Misfit layer compounds (MLCs) prepared using the same synthesis approach were subsequently shown to have similar ultra low thermal conductivities of (0.06 to 0.14) $W \cdot m^{-1}K^{-1}$.[10] The only prior report of the thermal conductivity of a MLC reported a significantly higher value, 0.8 $W \cdot m^{-1}K^{-1}$ for $[Yb_{0.95}S_1]_{1.24}NbS_2$.[11] The structure of MLCs lends itself to the type of turbostratic disorder found in WSe_2 and consequently ultra low thermal conductivity.

Misfit layer compounds containing interpenetrating layers of MX and TX_2 are a potentially large family of compounds having the general formula $[(MX)_{1+y}]_m(TX_2)_n$, where M=Sn, Pb, Sb, Bi, and rare earth metals; T=Ti, V, Cr, Nb, Ta; and X=S and Se.[12-17] The values of *m* and *n*, respectively, represent the numbers of MX and TX_2 layers in the unit cell. Each TX_2 layer consists of a hexagonal layer of metal T between hexagonal planes of chalcogen with the T atoms in trigonal prisms of X. Each MX layer contains two distorted 001 planes of the rock salt structure. The rock salt structured layers contain equal amounts of M and X atoms and are incommensurate with the close packed X planes of the chalogen layers of TX_2. The misfit parameter, *y*, describes the difference between the density of metal cations in their respective layers. The range of *y* reported in the literature is from 0.07 to 0.28.[18, 19] Prior reports on these compounds have focused on the unusual crystal structures resulting from the misfit between the two sublattices and the broad range of physical properties observed in MLCs.[13, 20] High temperature synthesis has been used to prepare these compounds, typically resulting in the formation of the simplest compound of the family, with $m = n = 1$, as an ordered three-dimensional solid. The synthetic challenge is that many potential members of this class of compounds are metastable with respect to either the binary compounds, the $m = n = 1$ compound or other ternary compositions. To fully exploit the unusual structure and physical properties of this class of materials, a general route to families of these metastable compounds is required.

In this paper we describe a general strategy for the synthesis of layered compounds with incommensurate structures and use this approach to prepare the first 64 members, denoted (*m*, *n*), of the family $[(PbSe)_{0.99}]_m(WSe_2)_n$ ($1 \le m, n \le 8$) of ultra low thermal conductivity MLCs. Figure 1 contains a schematic of the free energy versus composition for a family of MLCs that asserts that each distinct compound (*m*, *n*) is at least a local free energy minimum. Our synthesis approach is to prepare a precursor at low temperature that has enough similarities to the structure of the desired product that low temperature annealing results in the self-assembly of the desired compound as it is trapped in the local free energy minima. The results presented here suggest that it is sufficient to sequentially deposit a pair of elemental layers for each constituent where the ratio of the elements corresponds to the stoichiometric ratio found in each of the constituents and the thickness of the pair of elemental layers corresponds to the absolute amount of material required to make a single layer of each constituent. We demonstrate that by depositing *m* layers of Pb-Se and *n* layers of W-Se in this manner, the (*m*, *n*) family member forms on low temperature annealing. This approach does not require an epitaxial relationship between film and substrate, overcoming the limitations imposed by epitaxial growth conditions. This is the first report of the synthesis of a large number of misfit layer compounds in a single family.

Experimental section

The samples were prepared in a custom-built high vacuum deposition system described elsewhere.[21] The tungsten and lead were deposited with an electron beam gun at a rate (0.02 and 0.04) nm/s respectively, and selenium was deposited with an effusion cell at a rate of 0.05 nm/s. A quartz crystal monitoring system placed 25 cm above each source was used to control deposition rates and the length of time a shutter was left open to control elemental layer thicknesses. The sample precursors were deposited onto (100) silicon wafers at ambient

temperature for X-ray diffraction (XRD) and X-ray reflectivity (XRR) studies, and onto polished fused silica slides for electrical measurements. XRD and XRR measurements indicate that films deposited onto fused silica substrates are typically rougher, but otherwise structurally similar to those deposited onto silicon substrates. The precursors were prepared by depositing *m* repetitions of (Se-Pb) followed by *n* repetitions of (Se-W) and repeating this sequence until a total thickness in the range of (20 to 200) nm was obtained. Deposition parameters were determined to yield the appropriate stoichiometry and absolute number of atoms required for a PbSe rock salt bilayer or a Se-W-Se dichalcogenide trilayer, respectively. Samples were annealed at 400 °C for 1 h under an inert nitrogen atmosphere to crystallize the samples.

Chemical composition was determined using a Cameca S-50 electron probe microanalyzer (EPMA) and the Stratagem data analysis program* using a beam current of 20 nA and beam voltages of (8, 12, and 16) kV. X-ray wavelength dispersive spectrometry was performed using pure elements or compounds as standards. Ten independent measurements at different sample positions were averaged to determine the final composition.

The crystalline quality, orientation, and thickness of the films were evaluated by high resolution X-ray diffraction and reflectivity using a Bruker D8 Discover diffractometer with Cu $K_{\alpha 1}$ radiation and Göbel mirror, Bragg-Brentano Optics Geometry. X-ray powder diffraction patterns were also measured in the high resolution 33ID beam line of the Advanced Photon Source (APS) at Argonne National Laboratory. The sample was mounted on 4-circle Huber goniometer. All a-lattice and b-lattice parameters of the film were calculated from in-plane XRD data at APS. Two dimensional (2D) k-space mapping was performed using a Marresearch GmbH MAR345 image plate detector at a grazing incidence angle of 1.0º. In the synchrotron experiments, two wavelengths of (95.78 and 94.29) pm were used for anomalous XRD scans and a wavelength of 92.53 pm was used for in-plane XRD. The diffraction data collected at different energies were refined using the General Structure Analysis System (GSAS). Several XRD patterns for samples of $[(PbSe)_{0.99}]_m(WSe_2)_n$ were collected for Rietveld refinement analysis in the range $12^o \leq 2\theta \leq 50^o$ with a step increment of 0.005^o and 1s acquisition per step. The analyses based on Rietveld refinement have about 2 % error.

Cross section specimens for scanning (STEM) and conventional (TEM) transmission electron microscopy analysis were prepared using the small angle cleavage technique (SACT),[22] followed by cleaning and thinning using a FEI NOVA NanoLab DualBeam FIB equipped with a Sidewinder ion column. Samples were thinned to approximately 300 nm using 30 kV accelerating voltage on the ion source followed by a polishing step at 5 kV and final endpointing at 2 kV. Samples were plasma cleaned using a Fischione Instruments model 1020 plasma cleaner for 5 min prior to analysis to remove any organic contamination.

Analytical electron microscopy measurements were performed using an FEI Titan STEM/TEM equipped with a double-hexapole spherical aberration (C_s) corrector on the probe forming lens and operating at 300 kV. Images were collected using a condenser beam convergence semi-angle α = 18 mrad and a high angle annular dark-field (HAADF) detector with an inner semi-angle of β = 60 mrad. Imaging was conducted by first orienting the specimen to the [110] zone axis of the silicon substrate, followed by a lateral stage shift to the site of interest. Orientation at the [110] zone axis of silicon places the cross section of the film normal to the optic axis of the microscope. STEM-HAADF images were acquired with a 4pi RevolutionSEM™ digital imaging system, which allowed the integration of multiple scan frames following drift correction. The resulting images exhibit high signal-to-noise and negligible distortion arising from specimen drift during image collection. Image analysis was conducted using the ImageJ for Microscopy suite of plug-ins.[23, 24] Distances were measured using the line tool and the plot profile feature on the calibrated image. A large line width was chosen to provide an average

* Certain commercial equipment, instruments, or materials are identified in the document. Such identification does not imply recommendation or endorsement by the National Institute of Standards and Technology, nor does it imply that the products are necessarily the best available for the purpose.

distance over many atomic columns. Special care was taken to ensure that the line was perpendicular to the film cross section during the measurement.

Raman spectroscopy measurements were conducted on several compounds, (*m*, *n*), in the family to study the charge transfer and interlayer interaction between the two constituents. The spectra were measured at room temperature. The excitation wavelength of the incident radiation was 541.532 nm from an Ar laser. The laser spot on the sample surface was ≈ 1 μm diameter. The experiments were performed in parallel (xx) and crossed (xy) polarization geometries. The directions of the incident and scattered radiation were parallel to the z-direction (c-axis of the crystal).

Results and discussions

Figure 2 contains a schematic of the precursor designed to evolve into the (1,1) compound, the simplest member in this MLC family. In constructing the precursor, both the local composition and absolute number of atoms deposited in each layer are important. To form the desired MLC, it is necessary that the ratio of the deposited elements in the Pb-Se and W-Se pair of elemental layers correspond to the stoichiometry of the desired PbSe and WSe_2 constituents respectively. The absolute amount of each of the elements in the Pb-Se and W-Se layers must correspond to the number of atoms required to form precisely two atomic layers of (001)-oriented rock salt structured PbSe and a Se-W-Se dichalcogenide trilayer sandwich, respectively. To accomplish this, we determined the empirical relationship between the ratio of the deposition thickness (the product of the deposition rate of each source and the time the shutter is kept open, which is proportional to the actual layer thickness) for each pair of elements and the resulting composition ratio of the elements for each Pb/Se and W/Se pair. This calibration, shown in Figure 3 for Pb-Se, accounts for the geometry of the deposition system, differences in sticking coefficients and the difference in placement between the deposition monitors and the samples. The linear relationship between the atomic ratio and the thickness ratio is used to determine the conditions required to obtain the desired composition. Using the thickness ratio that gives the desired composition, a second set of samples is prepared to confirm that the sample composition remains constant as the deposition times are varied while maintaining the same thickness ratio. The actual thickness of each of the bilayer samples was measured experimentally by XRR both before and after annealing to high enough temperatures to crystallize the desired MLC. These data are used to determine the extent of densification as the films crystallize, enabling us to approximately deposit the amount of each pair of elements required to form one Se-W-Se trilayer and one bilayer of (001)-oriented PbSe.

To optimize the absolute amount of each component required to form the targeted (1,1) compound, a third set of calibration samples was prepared. In one sequence of samples the number *m* of Pb-Se bilayers was held constant while the number *n* of W-Se trilayers was systematically changed. A second set of samples was prepared where the number *n* of W-Se trilayers was held constant while the number *m* of Pb-Se bilayers was varied. The data in Figure 4 give a best fit of $(\partial c/\partial n)_m = 0.660$ nm, where *c* is the thickness of the repeating unit. The slope corresponds to the average thickness of each W-Se bilayer, which is slightly thicker than the thickness of a WSe_2 layer (0.655 nm) found in the binary compound WSe_2. The measured intercept of 0.640 nm is thicker than the unit cell size for rock salt structured PbSe reported in literature. A second sequence of samples was prepared, adjusting the repeat thickness of the bilayer that forms each component so their thicknesses are within 0.005 nm of the c-axis lattice parameters for the parent hexagonal WSe_2 and rock salt PbSe compounds reported in the literature. Finally, small adjustments were made in the elemental layer thicknesses and correlated to the quality of the resulting X-ray diffraction patterns of the crystallized compounds. A slight excess of (1 to 2) % of selenium resulted in the most intense diffraction maxima with the smallest line widths.

X-ray diffraction data collected as a function of annealing temperature and time were used to optimize the annealing conditions and better understand the formation mechanism of the targeted MLCs. Figure 5 contains diffraction data collected from a precursor designed to form the (1,1) compound as a function of annealing temperature. The low angle XRD pattern of the as-deposited sample contains the expected Bragg peak resulting from the layered nature of the as-deposited precursor and the interference pattern resulting from its finite thickness (Kiessig fringes). The high angle diffraction pattern of the as-deposited precursor contains no observable Bragg peaks, reflecting its amorphous nature. Annealing the precursor results in a shift in the low angle Bragg peak to higher angle and the appearance of *00l* Bragg peaks as the (1,1) compound forms. The intensities of the Bragg maxima increase and the peak widths decrease as the annealing temperature is increased. The c-axis lattice parameter continuously decreases with annealing from (1.369 ± 0.004) nm at 200 ºC to (1.270 ± 0.001) nm at 400 ºC as the structure evolves. The lattice parameter remains constant at 1.270 nm after annealing at 500 °C, suggesting that the structure has reached a stable configuration. After annealing at 400 °C for 1 h, the Kiessig fringes extend out to $2\theta = 23º$, implying that the film is very smooth with near atomically flat interfaces. Using the relationship developed by Parratt,[25] the roughness was calculated to be ≈ 0.19 nm, a significant reduction relative to the ≈ 1.2 nm determined for the as-deposited film. The significant increase in smoothness of the films after annealing results from the two-dimensional growth habit of the MLC, leading to very parallel top and bottom surfaces of the film. While PbSe and WSe_2 do not exhibit an epitaxial relationship, the diffraction data suggest that the interfaces between them are nearly atomically smooth. The presence of only the *00l* family of peaks in the diffraction spectrum indicates a preferred crystallographic orientation of the crystalline (1,1) compound, with the crystallographic a-b plane parallel to the substrate. The preferred crystallographic alignment was quantified by rocking curve scans of the *002* and *004* Bragg peaks as a function of annealing temperature. The rocking-curve peak widths decrease from 2.7º in the as-deposited film to 0.53º after annealing at 400 ºC. The preferred growth of crystallites with this orientation is favored by the layered structure of the precursor as growth requires only small diffusion distances.

Once we determined the deposition parameters to form the (1,1) compound, the other higher order members of family (*m*, *n*) were prepared by depositing precursors containing *m* Pb-Se layers and *n* W-Se layers in a repeating unit. The number of repeating units can be increased to obtain the desired film thickness or mass of final product. Annealing the precursors under similar conditions required to form the (1,1) compound yielded the first 64 members of the family ($1 \leq m, n \leq 8$). The diffraction patterns exhibiting the highest peak intensities and the largest number of diffraction peaks resulted after annealing at 400 ºC for 1 h. Figure 6(a) contains the diffraction patterns of the compounds (1, *n*) with ($1 \leq n \leq 8$) where all of the diffraction maxima can be indexed as *00l* Bragg reflections. The c-axis lattice parameter systematically changes as either *m* or *n* is increased within this family of compounds as shown in Figure 6(b). The slopes vary between (0.654 and 0.656) nm and the intercepts, normalized by the thickness of the rock salt layer *m*, vary between (0.612 and 0.615) nm. The slope reflects the thickness, c', of the dichalcogenide trilayer within the structure, and the value is in agreement with the values ($0.647 \text{ nm} \leq c' \leq 0.662 \text{ nm}$) for individual Se-W-Se layers reported for polytypes of WSe_2.[26-28] The intercepts correspond to the thickness of the PbSe bilayer and are consistent with the (0.611 to 0.614) nm variation observed for bulk FCC PbSe.[29, 30] These systematic changes and agreement with the literature support the values of *m* and *n* assigned to each compound and are consistent with the predicted free energy minima for integer values of *m* and *n*, as shown in Figure 1. The compositions of the samples (*m*, *n*) as measured by electron microprobe are in agreement, within the measurement uncertainty, with that calculated for these compounds. We have not explored the maximum values of *m* and *n* that can be prepared using this approach.

The formation of the MLCs containing both PbSe and WSe_2 structural units is also clearly observed in the in-plane XRD patterns. Figure 7 shows in-plane XRD data of the (2,2) compound, where the *hk0* Bragg peaks for

each of the independent structural units are observed and can be indexed independently. The difference in peak profiles result in the striking difference in in-plane coherence length; the approximately 8.2 nm in-plane coherence within PbSe is much larger than approximately 4.0 nm in-plane coherence within WSe_2. The a-axis lattice parameters obtained, (0.331 ± 0.001) nm for the WSe_2 structural unit and (0.6182 ± 0.0002) nm for the PbSe structural unit, are both slightly larger than the values reported for the binary compounds, 0.3255 nm for WSe_2[31] and 0.6121 nm for PbSe.[29] The PbSe structural unit appears to be distorted from cubic to tetragonal using the estimated c-axis lattice parameter of (0.612 to 0.615) nm. No significant change (< 0.2 %) in lattice parameters in the a-b plane is observed when varying the values of indices *m* and *n*. By calculating the areas of the structural unit cell sizes of both components, we observed that the number density of Pb atoms was 1.0 % smaller than the number density of W atoms in the a-b plane, corresponding to a value of the misfit parameter $y = -0.01$. This is the first negative value of the misfit parameter *y* reported to date for a chalcogen-based misfit layer compound.

Rietveld refinements of the *00l* diffraction pattern of the (1,1) compound at X-ray wavelengths above and below the Pb L_3 edge, shown in Figure 8, reveal an arrangement of atoms along the c axis consistent with previously reported MLC structures. The (1,1) compound is built of a bilayer of PbSe (approximately two 001 atomic planes of PbSe with a rock salt structure) alternating with a WSe_2 dichalcogenide trilayer. The structures of the constituent layers are considerably distorted from the arrangement found in the binary compounds. The Pb and Se atoms in the distorted rock salt strucutred layer are no longer planar, with the Pb atoms closer to the selenium of the tungsten diselenide by 0.023 nm. This puckering of what would be a plane of Pb and Se in an interpenetrating square lattice is within the 0.002 nm to 0.08 nm range previously reported for this distortion in MLCs.[32-36] The distortion is a consequence of the lead completing its local coordination through bonding to the selenium of the dichalcogenide layer. The Pb-Se bond distance between the layers of the PbSe double layer is found to be 0.259 nm, significantly shorter than the 0.306 nm found in bulk PbSe. The distance defined by the average rock salt position to the Se in the dichalcogenide is 0.365 nm, the same as the reported literature value for the van der Waals gap in WSe_2.[37] The WSe_2 structural unit was found to be similar to that observed in the binary compound. The intralayer distance between W and the Se layers is 0.141 nm, considerably larger than the 0.126 nm reported in the literature for bulk WSe_2,[37] as a consequence of the interaction between the PbSe and WSe_2 components of the structure. The possible extent of W-Pb intermixing was probed by refining the structure using diffraction data collected above and below the Pb L_3 edge. While previous reports have indicated as much as (5 to 20) % mixing of the cations,[15] refinement allowing the cations to mix resulted in only (4 ± 2) % of Pb on the W sublattice of the dichalcogenide and (3 ± 2) % of W on the Pb sublattice of the rock salt.

Figure 9 shows a STEM-HAADF (Z-contrast) image of the (2,1) compound that shows a repeating structure of two bilayers (four atomic planes) of PbSe interspersed by single WSe_2 trilayers. The c-axis lattice parameter from the image is in agreement with the value obtained by XRD. A striking feature of Figure 9 is the variation of the orientation of the PbSe structural units within the superlattice structure. Structural domains can be seen with a <100> zone axis orientation, a <110> zone axis orientation, and not along any particular zone axis, <hk0>, all adjacent to one another. Changes in orientation are observed both upon crossing a WSe_2 layer (interlayer) and within individual layers (intralayer). A similar rotational disorder may be present in the WSe_2 layers. The presence of layers with different a-b axis orientation while maintaining a common c axis confirm a turbostratic disorder in these compounds, which has been proposed as an explanation for their ultra-low c-axis thermal conductivity, ranging from 0.15 $Wm^{-1}K^{-1}$ for the (4,1) compound to 0.06 $Wm^{-1}K^{-1}$ for the (1,4) compound.[10] These thermal conductivities are an order of magnitude lower than the 0.8 $Wm^{-1}K^{-1}$ reported for $[Yb_{1.90}S_2]_{0.62}NbS_2$, the only previous report on the lattice thermal conductivity of a MLC.[11]

To further characterize the coherence and the degree of turbostratic disorder of these misfit layer compounds,

we collected XRD data throughout reciprocal space on several of the samples using a 2D image plate detector at the APS. Many *00l* reflections were found for all of the compounds investigated, reflecting the long-range order along the c axis. Scans collected with the correct geometry revealed many *hk0* reflections, again reflecting the long-range order in the a-b plane. Data collected with a sample orientation to obtain arbitrary *hkl* (i.e., $h+k\neq 0$; $l\neq 0$) reflections, however, revealed that the FWHM of *hkl* diffraction peaks are considerably broader than *hk0* or *00l* peaks, indicating a much shorter coherence length.[38] Weak satellite diffraction peaks corresponding to the superlattice structure could be indexed based on the values of lattice parameters determined from in-plane and cross plane diffraction data. The large line widths indicated that limited interlayer crystallographic ordering occurs, consistent with the turbostratic disorder seen in the STEM images. In summary, XRD suggests that the MLCs, (*m*, *n*), prepared in this study consist of regularly spaced layers along the c axis which exhibit rotational (turbostratic) disorder within the a-b planes.

The long-range order along the c axis and locally within the a-b planes, together with the relatively high kinetic stability of the different family members (*m*, *n*), suggest strong interactions between the layers that compensate for the low entropy inherent to such an ordered stacking. Since these compounds are built up of two sub-systems that have different chemical compositions, geometric structure and symmetry and a lack of lattice matching, the observed rotational disorder between layers might lower the free energy without sacrificing much enthalpy. Generally, the overall stability of the MLC structures is explained by charge transfer between the MX and the TX_2 sub-system and has been assessed by means of theoretical calculations,[39] x-ray photoelectron spectroscopy[40] and Raman scattering.[41, 42] On the basis of initial density functional theory (DFT) calculations performed with Wien2K on an idealized structure model, we find a small charge transfer from the WSe_2 to the PbSe layers as the interlayer separation is decreased below approximately 0.4 nm. This result is consistent with the Pb-Se interlayer interaction, which preferentially draws electron density from the WSe_2 layer. In addition, total-energy, semiempirical calculations on capped, isolated PbSe layers are consistent with the observed buckling of the a-b plane, indicating that formation of the interlayer Pb-Se interaction promotes the buckling of the layers. We also used Raman scattering to assess the bonding between PbSe and WSe_2 in several (*m*, *n*) compounds. The A_{1g} (off-plane) and E_{2g} (in-plane) phonon modes of the dichalcogenide layer can be observed in all samples measured, and the phonon energies do not depend on the values of *m* or *n*. The Raman band in the z(xx)z-spectrum at 250 cm^{-1} was assigned to the A_{1g} mode, the direction of displacement vectors being perpendicular to the WSe_2 layer, and two overlapping Raman bands in the z(xy)z-spectrum at (250 and 220) cm^{-1} were assigned to A_{1g} and E_{2g} modes, the displacement vectors being parallel to the WSe_2 layer. The A_{1g} and E_{2g} phonon energies of the MLCs were smaller than those of the bulk WSe_2 phonon energies A_{1g} = 253 cm^{-1} and E_{2g} = 250 cm^{-1}, respectively. The Raman shift in observed phonon energy is 1 % for A_{1g} and 12 % for E_{2g}. These results are consistent with reported Raman measurements on other MLCs where the frequency of E mode was found to shift (10 to 20) %, while that of the A modes remain unchanged relative to the corresponding binary dichalcogenide compound.[14, 41, 43-45] The small phonon frequency shift suggests a relatively weak interlayer interaction between WSe_2 and PbSe layers and a small amount of charge transfer between layers, consistent with that observed in $(SnS)_{1+y}(TS_2)_n$ and $(PbS)_{1+y}(TS_2)_n$ MLCs with T=Nb, Ta and Ti.[46, 47] The shifts in the phonon energies for the WSe_2 layers relative to the bulk are also consistent with the transfer of charge from the WSe_2 layers in our initial calculations.

Conclusions

We have successfully fabricated a family of new misfit layer compounds, $[(PbSe)_{0.99}]_m(WSe_2)_n$ ($1 \leq m, n \leq 8$), by a multilayer thin film deposition technique that combines solid state reactions of elemental reactant layers in a

designed precursor and relatively low temperature annealing to self-assemble the desired compound. The self-assembly results in preferred crystallographic alignment, with the c-axis of the rock-salt- and dichalcogenide structural units perpendicular to the substrate, and in films with exceptionally uniform thickness. The structure of the misfit layer compounds prepared using this approach is neither completely crystalline nor completely amorphous. Long-range order is found along the c-axis and within the a-b plane of each of the constituents. There are significant structural distortions in the constituents, relative to the structures of the corresponding bulk binary compounds, reflecting the interactions between them that stabilize the kinetically trapped structures. There is a rotational or turbostratic disorder between the crystallographic orientations of the constituents. This disorder is thought to result in the ultra-low thermal conductivity of this family of compounds, which makes them attractive candidates for application in the thermal barrier coatings and thermoelectric energy conversion technologies. This synthesis method, based on preparing a designed precursor that self assembles into the desired family member, may provide a general approach to other misfit layer compounds with low thermal conductivity and to more complicated compounds consisting of three interwoven components with different repeat patterns such as $A_xB_yC_z$, $A_xB_yC_zB_y$, providing an opportunity to tune a variety of interesting and potentially useful physical and chemical properties.

Acknowledgements

This work was supported through the Office of Naval Research (N0014-07-1-0358). Coauthors CLH and MDA were supported by the National Science Foundation through the IGERT grant (DGE-0549503). The use of the APS was supported by the U.S. Department of Energy, Office of Science, Office of Basic Energy Sciences, under contract number DE-AC02-06CH11357. Coauthors RK and DAK acknowledge support from the National Science Foundation through CCI grant number CHE-0847970. We wish to acknowledge and thank Dr. Andrew Herzing of NIST for help with acquiring the high-resolution STEM images.

References

1. Bell, L. E. *Science* **2008,** *321*, 1457-1461.
2. Snyder, G. J.; Toberer, E. S. *Nature Mater.* **2008,** *7*, 105-114.
3. Padture Nitin, P.; Gell, M.; Jordan Eric, H. *Science* **2002,** *296*, 280-284.
4. Uzun, A.; Cevik, I.; Akcil, M. *Surf. Coat. Technol.* **1999,** *116-119*, 505-507.
5. Gurrappa, I.; Rao, A. S. *Surf. Coat. Technol.* **2006,** *201*, 3016-3029.
6. Li, S.; Funahashi, R.; Matsubara, I.; Ueno, K.; Sodeoka, S.; Yamada, H. *Chem. Mater.* **2000,** *12*, 2424-2427.
7. Hsu, K. F.; Loo, S.; Guo, F.; Chen, W.; Dyck, J. S.; Uher, C.; Hogan, T.; Polychroniadis, E. K.; Kanatzidis, M. G.. *Science* **2004,** *303*, 818-821.
8. Poudel, B.; Hao, Q.; Ma, Y.; Lan, Y.; Minnich, A.; Yu, B.; Yan, X.; Wang, D.; Muto, A.; Vashaee, D.; Chen, X.; Liu, J.; Dresselhaus, M. S.; Chen, G.; Ren, Z. *Science* **2008,** *320*, 634-638.
9. Chiritescu, C.; Cahill, D. G.; Nguyen, N.; Johnson, D.; Bodapati, A.; Keblinski, P.; Zschack, P. *Science* **2007,** *315*, 351-353.
10. Chiritescu, C.; Cahill, D. G.; Heideman, C.; Lin, Q.; Mortensen, C.; Nguyen, N. T.; Johnson, D.; Rostek, R.; Bottner, H. *J. Appl. Phys.* **2008,** *104*, 033533/1-033533/5.
11. Miyazaki, Y.; Ogawa, H.; Kajitani, T. *Jpn. J. Appl. Phys.* **2004,** *43*, L1202-L1204.
12. Moelo, Y.; Meerschaut, A.; Rouxel, J.; Auriel, C. *Chem. Mater.* **1995,** *7*, 1759-1771.
13. Wiegers, G. A. *Prog. Sol. State Chem.* **1996,** *24*, 1-139.
14. Ohno, Y.; Shimokawa, S. *J. Sol. State Chem.* **2004,** *177*, 2818-2826.

15. Kallane, M.; Rossnagel, K.; Marczynski-Buhlow, M.; Kipp, L.; Starnberg, H. I.; Stoltz, S. E. *Phys. Rev. Lett.* **2008,** *100*, 065502.

16. Hernan, L.; Morales, J.; Sanchez, L.; Santos, J.; Rodriguez-Castellon, E.; Martinez, J. L. *Chem. Mater.* **2000,** *12*, 3792-3797.

17. Szabo, P.; Samuely, P.; Kacmarcik, J.; Jansen, A. G. M.; Briggs, A.; Lafond, A.; Meerschaut, A. *Phys. Rev. Lett.* **2001,** *86*, 5990-5993.

18. Gotoh, Y.; Onoda, M.; Akimoto, J.; Goto, M.; Oosawa, Y. *Jpn J. Appl. Phys.* **1992,** *31*, 3946-3950.

19. Lafond, A.; Deudon, C.; Meerschaut, A.; Sulpice, A. *Eur. J. Sol. State Inorg. Chem.* **1994,** *31*, 967-978.

20. Rouxel, J.; Moeelo, Y.; Lafond, A.; DiSalvo, F. J.; Meerschaut, A.; Roesky, R. *Inorg. Chem.* **1994,** *33*, 3358-3363.

21. Fister, L.; Li, X.-M.; McConnell, J.; Novet, T.; Johnson, D. C. *J. Vac. Sci. Technol. A* **1993,** *11*, 3014-3019.

22. Walck, S. D.; McCaffrey, J. P., *Thin Solid Films* **1997,** *308-309*, 399-405.

23. Rasband W.S., *National Institutes of Health, Bethesda, Maryland, USA, http://rsb.info.nih.gov/ij/,* **1997-2004**.

24. Thévenaz, P.; Ruttimann, U. E.; Unser, M. *IEEE Trans. Image Process.* **1998,** *7*, 27-41.

25. Wainfan, N.; Parratt, L. G. *J. Appl. Phys.* **1960,** *31*, 1331-1337.

26. Coehoorn, R.; Haas, C.; Dijkstra, J.; Flipse, C. J. F.; De Groot, R. A.; Wold, A. *Phys. Rev. B* **1987,** *35*, 6195-6202.

27. Voss, D.; Kruger, P.; Mazur, A.; Pollmann, J. *Phys. Rev. B* **1999,** *60*, 14311-14317.

28. Finteis, T.; Hengsberger, M.; Straub, T.; Fauth, K.; Claessen, R.; Auer, P.; Steiner, P.; Hufner, S.; Blaha, P.; Vogt, M.; Lux-Steiner, M.; Bucher, E., *Cond. Matter Mater. Phys.* **1999,** *59*, 2461.

29. Wei, S.-H.; Zunger, A. *Phys. Rev. B* **1997,** *55*, 13605.

30. Hummer, K.; Gruneis, A.; Kresse, G.. *Phys. Rev. B* **2007,** *75*, 195211/1-195211/9.

31. Sharma, S.; Ambrosch-Draxl, C.; Khan, M. A.; Blaha, P.; Auluck, S. *Phys. Rev. B* **1999,** *60*, 8610-8615.

32. Oosawa, Y.; Gotoh, Y.; Akimoto, J.; Tsunoda, T.; Sohma, M.; Onoda, M. *Jpn J. Appl. Phys.* **1992,** *31*, L1096- L1099.

33. Gotoh, Y.; Onoda, M.; Akimoto, J.; Oosawa, Y. *Jpn J. Appl. Phys.* **1991,** *30*, L1039-L1041.

34. van Smaalen, S.; Petricek, V. *Acta Cryst. A* **1992,** *48*, 610-618.

35. Wiegers, G. A.; Meetsma, A.; De Boer, J. L.; Van Smaalen, S.; Haange, R. J. *J. Phys. Cond. Matter* **1991,** *3*, 2603-2612.

36. Wiegers, G. A.; Meetsma, A.; Haange, R. J.; De Boer, J. L. *J. Sol. State Chem.* **1990,** *89*, 328-339.

37. Schutte, W. J.; De Boer, J. L.; Jellinek, F. *J. Sol. State Chem.* **1987,** *70*, 207-209.

38. Zschack, P.; Heideman, C.; Mortensen, C.; Nguyen, N.; Smeller, M.; Lin, Q.; Johnson, D. C. *J. Electron. Mater.* **2009,** *38*, 1402-1406.

39. Fang, C. M.; Ettema, A. R. H. F.; Haas, C.; Wiegers, G. A.; van Leuken, H.; de Groot, R. A. *Phys. Rev. B* **1995,** *52*, 2336.

40. Ettema, A. *J. Phys. Cond. Matter* **1993,** *5*, 3817.

41. Hangyo, M.; Nakashima, S.; Hamada, Y.; Nishio, T.; Ohno, Y. *Phys. Rev. B* **1993,** *48*, 11291-11297.

42. Kisoda, K.; Hangyo, M.; Nakashima, S.; Terashima, T.; Kojima, N. *Physica B* **1996,** *219-220*, 565-567.

43. Kisoda, K.; Hangyo, M.; Nakashima, S.; Suzuki, K.; Enoki, T.; Ohno, Y. *J. Phys. Cond. Matter* **1995,** *7*, 5383-5393.

44. Sourisseau, C.; Cavagnat, R.; Fouassier, M.; Tirado, J. L.; Morales, J. *Chem. Phys.* **1994,** *181*, 377-392.

45. Shirai, K.; Kisoda, K.; Hangyo, M.; Nakashima, S. *Sol. State Comm.* **1997,** *103*, 131-135.

46. Fang, C. M.; Wiegers, G. A.; Meetsma, A.; de Groot, R. A.; Haas, C. *Physica B* **1996,** *226*, 259-267.

47. Fang, C. M.; de Groot, R. A.; Wiegers, G. A.; Haas, C. *J. Phys. Cond. Matter* **1996,** *8*, 1663-1676.

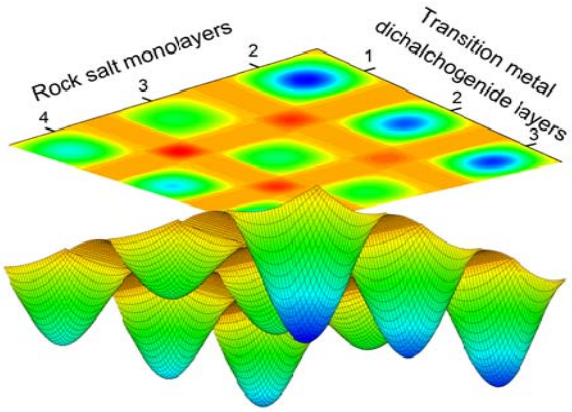

Figure 1. Schematic multi-minima free energy hypersurface of a potential misfit layer compound system, containing interwoven layers of rock salt and dichalcogenide layers. We show that each integer value of the respective constituent layers defines regions of composition-configuration space that are local free energy minima.

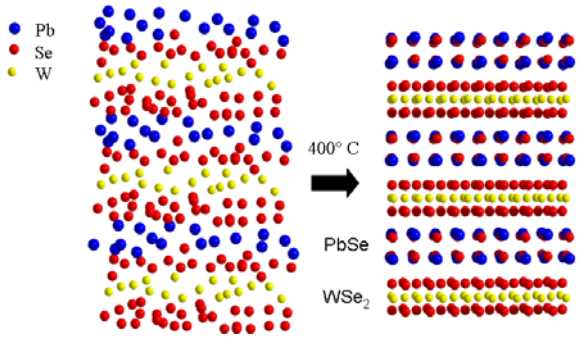

Figure 2. A schematic of the initial precursor prepared to make the misfit layer compound $[(PbSe)_{0.99}]_1(WSe_2)_1$ and the proposed structure after annealing at 400 ºC for 1 h.

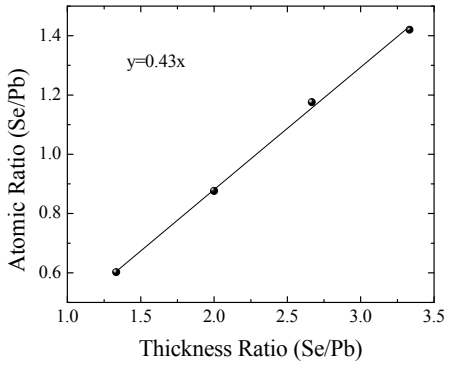

Figure 3. Graph of the atomic ratio of Pb and Se determined from EPMA versus the ratio of the deposition thicknesses of Pb and Se for a series of binary calibration samples.

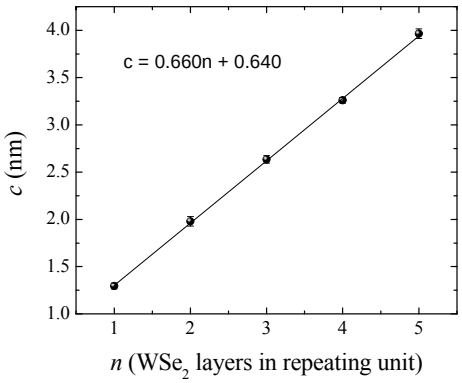

Figure 4. The measured thickness of the repeat structure in the precursor is plotted as a function of the number of W-Se bilayers deposited in the repeat structure. The slope is the thickness of each W-Se bilayer deposited and the intercept is the thickness of the Pb-Se bilayer.

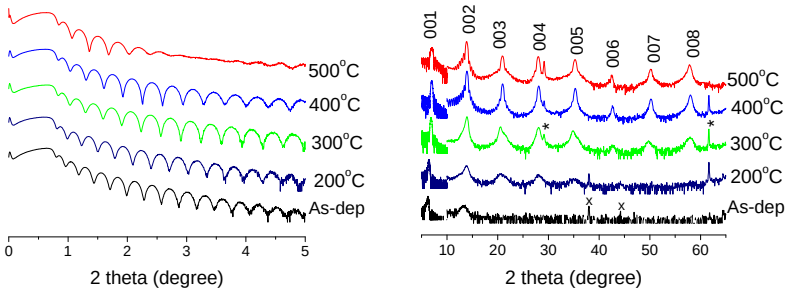

(a) (b)

Figure 5. The evolution of (a) low angle and (b) high angle XRD data as a function of annealing temperature of a precursor designed to crystallize into $[(PbSe)_{0.99}]_1(WSe_2)_1$. The sample was annealed under N_2 environment with an O_2 concentration of less than 0.5 μL L^{-1} for 1 h at each temperature. Silicon peaks (002) and (004) at 2θ = (29.5º and 61.9º) respectively arise from the substrate and are denoted by (*); boron carbide (PDF# 86-1117) peaks (113) and (006) at 2θ = (38.1º and 44.2º) respectively arise from the stage and are denoted by (x).

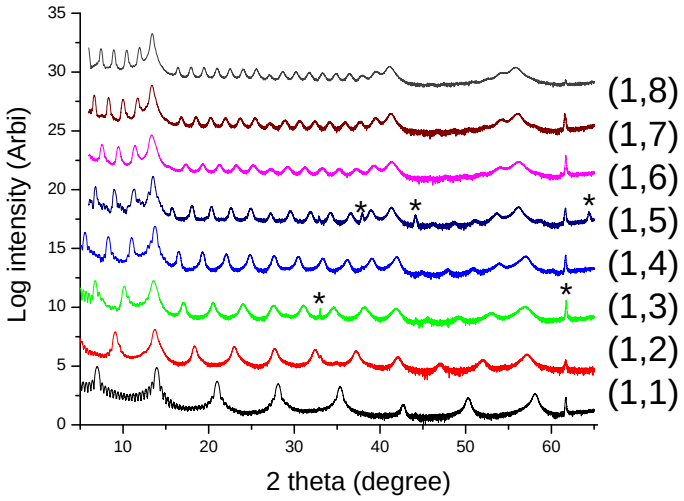

(a)

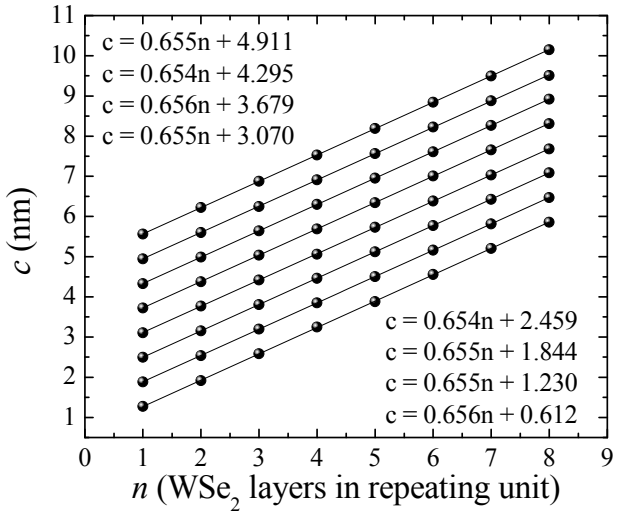

(b)

Figure 6. (a). XRD patterns using Cu Kα radiation for a sub-family of misfit layer compounds $[(PbSe)_{0.99}]_1(WSe_2)_n$, in which the number of lead selenide layers is held constant while the number of tungsten diselenide layers is varied. The compound name on right side of each curve is briefly expressed by (*m*, *n*). Asterisks indicate substrate or stage peaks. (b). A plot of the c lattice parameter as a function of n, the number of layers of WSe_2, for 64 members ($1 \leq m, n \leq 8$) of the MLC family of $[(PbSe)_{0.99}]_m(WSe_2)_n$ compounds.

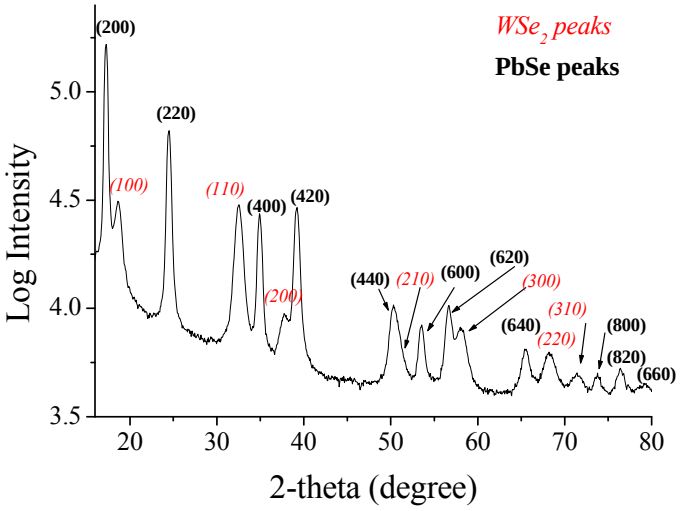

Figure 7. In-plane diffraction XRD for $[(PbSe)_{0.99}]_2(WSe_2)_2$ compound using an X-ray energy of 92.53 pm. All peaks can be indexed based on two independent sets of crystal structure of PbSe and WSe_2. The data were acquired with a synchrotron radiation source at the 33ID beam line at the APS.

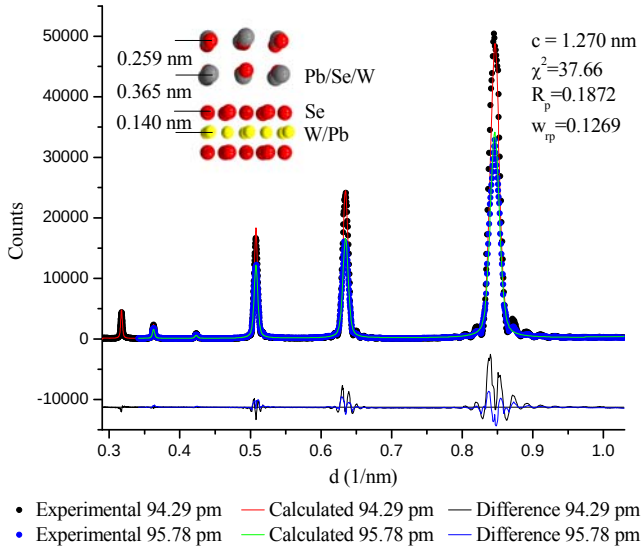

Figure 8. The Rietveld refinement results on $[(PbSe)_{0.99}]_1(WSe_2)_1$. The diffraction patterns measured with 2 different X-ray wavelengths, (95.78 and 94.29) pm, were compared with the misfit layer compound structural model by LeBail fitting. The refined c lattice parameter was 1.2697 nm. The bond distances are shown in the figure. The distortion of rock salt structure is $\delta = 0.025$ nm. The residuals $R_{wp} = 0.1872$, $R_p = 0.1269$ compare well with those obtained from the LeBail fit $R_{wp} = 0.1900$, $R_p = 0.1269$, and $\chi^2 = 37.66$.

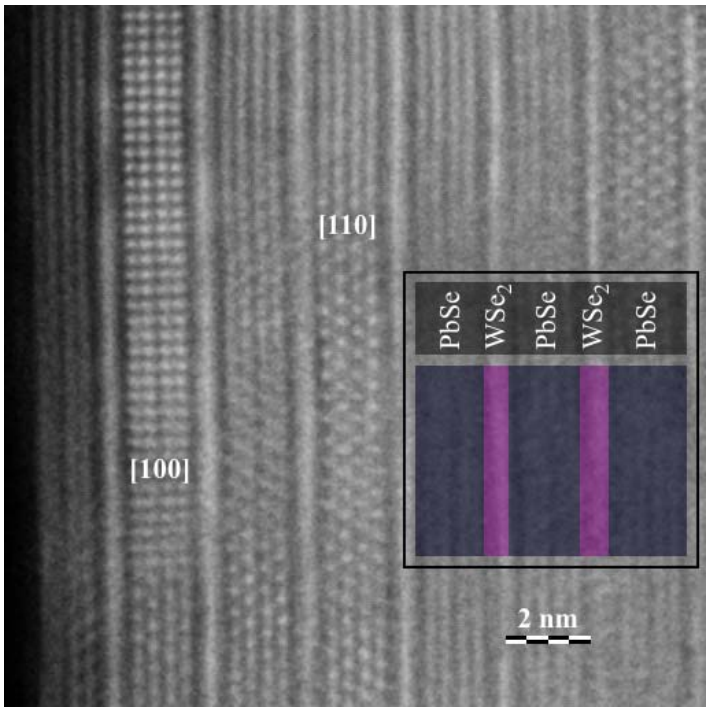

Figure 9. High resolution STEM Z-contrast image of a $[(PbSe)_{0.99}]_2(WSe_2)_1$ sample. The rock salt structured PbSe and dicalcogenide structured WSe_2 layers are distinct and regularly ordered. Rock salt structured domains exhibit numerous in-plane rotational variants, aligned along the <100> and <110> zone axes, as indicated, or along no major zone axis, <hk0>, of the structure.